Shape-Selective Zeolites for Tandem CO_2 Hydrogenation-Carbonylation Reactions

Hendrik Van Dessel,[a] Sam Van Minnebruggen,[a] Jasper Dedapper,[a] Paul Paciok,[b] Oleg Usoltsev,[c] Andraž Krajnc,[d] Aram Bugaev,[e] and Dirk E. De Vos*[a]

[a] H. Van Dessel, Dr. S. Van Minnebruggen, J. Dedapper and Prof. D. E. De Vos
Centre for Membrane Separations, Adsorption, Catalysis and Spectroscopy for Sustainable Solutions (cMACS) KU Leuven, Celestijnenlaan 200F p.o. box 2454, 3001 Leuven (Belgium) E-mail: dirk.devos@kuleuven.be

[b] Dr. P. Paciok Ernst Ruska-Center for Microscopy and Spectroscopy with Electrons and Peter Grünberg Institute, Forschungszentrum Julich 52425 Jülich (Germany)

[c] Dr. O. Usoltsev CELLS-ALBA Synchrotron Radiation Facility 08290 Cerdanyola del Vallès (Spain)

[d] Dr. A. Krajnc Department of Inorganic Chemistry and Technology, National Institute of Chemistry Hajdrihova 19, SI-1001 Ljubljana (Slovenia)

[e] Dr. A. Bugaev SuperXAS Beamline, Paul Scherrer Institute Forschungsstrasse 111, 5232 Villigen PSI (Switzerland)

Abstract: The valorization of carbon dioxide as a C1 building block in C-C bond forming reactions is a critical link on the road to carbon-circular chemistry. Activation of this inert molecule through reduction with H_2 to carbon monoxide in the reverse water-gas shift (RWGS) reaction can be followed by a wide spectrum of consecutive carbonylation reactions, but the RWGS is severely equilibrium limited at the moderate temperatures of carbonylations. Here we successfully reconcile both reactions in one pot, while avoiding incompatibilities through a zeolite-based compartmentalized approach. More specifically, Pt encapsulated in a small-pore LTA zeolite selectively generates carbon monoxide in mild reaction conditions; an ensuing one-pot carbonylation reaction allows to shift the equilibrium through continuous consumption of CO. Moreover, the zeolite encapsulation avoids undesired reactions like hydrogenation of the olefin reactant through a molecular sieving effect. This strategy was first studied in-depth for Rh-catalyzed olefin hydroformylation with CO_2/H_2, affording aldehydes in good yields with high regioselectivities. The methodology was then extended to a variety of carbonylations using CO_2 for the synthesis of bulk and fine chemicals.

Introduction

The excessive anthropogenic emission of CO_2 is a major global concern due to its significant contribution to global warming. Therefore, a drastic reduction in CO_2 and other greenhouse gas emissions is essential to meet climate commitments and keep our planet habitable.[1] In this context, the energy-efficient (re-)introduction of CO_2 in chemical building blocks represents an elegant strategy with dual benefit: mitigating environmental impact, while introducing oxygen-functionalities into base compounds to produce valuable chemicals.[2] Unfortunately, the inert nature of CO_2 hampers its direct use, often requiring the reduction to more reactive intermediates, e.g. carbon monoxide (CO), methanol

(CH_3OH) and formic acid (HCOOH). The reverse water-gas shift (RWGS) reaction is of particular interest in this regard, requiring only one molecule of H_2 to reduce CO_2 towards the more reactive CO, with water as the sole by-product. Moreover, CO is an important C1 building block in chemical industry, as illustrated by the hydroformylation of olefins to aldehydes, a large scale homogeneously catalyzed process with an annual production exceeding 10 Mton.[3] In addition, methanol carbonylation[4] (Cativa and Monsanto process) and the alkoxycarbonylation of olefins[5] (Lucite Alpha process) present other relevant industrial carbonylative transformations. Thus, the incorporation of CO, directly derived from CO_2, in organic compounds could be a promising technology for the valorization of CO_2.

Although appealing as a concept, the direct coupling of CO-generation through RWGS with a carbonylation reaction creates severe incompatibilities regarding their respective reaction conditions. More specifically, the RWGS is an endothermic equilibrium reaction requiring elevated temperatures (>300 °C) to reach high CO_2 conversions. In addition, during RWGS, heterogeneous metal catalysts activate H_2,[6] which is irreconcilable with the presence of unsaturated substrates used in carbonylation chemistry (e.g. olefins in hydroformylation and in alkoxycarbonylation). Hence, hydrogenation side reactions will inevitably result in undesired losses of the olefinic feedstock to unreactive alkanes. To tackle some of the aforementioned incompatibilities, several single-catalyst approaches have been proposed, in which CO_2 reduction and olefin carbonylation are performed by the same catalyst (Figure 1a). In this regard, $Ru_3(CO)_{12}$ as the sole catalyst, often in combination with an ionic liquid and additives, has been applied to a number of reductive, carbonylative transformations of CO_2.[7] Additionally, alternative reducing methods (e.g. using MeOH, hydrosilanes or photons)[7g,8,9] or additives (e.g. acetic anhydride)[10] have been used to facilitate the CO_2 reduction to CO in tandem carbonylation reactions. Finally, Leitner

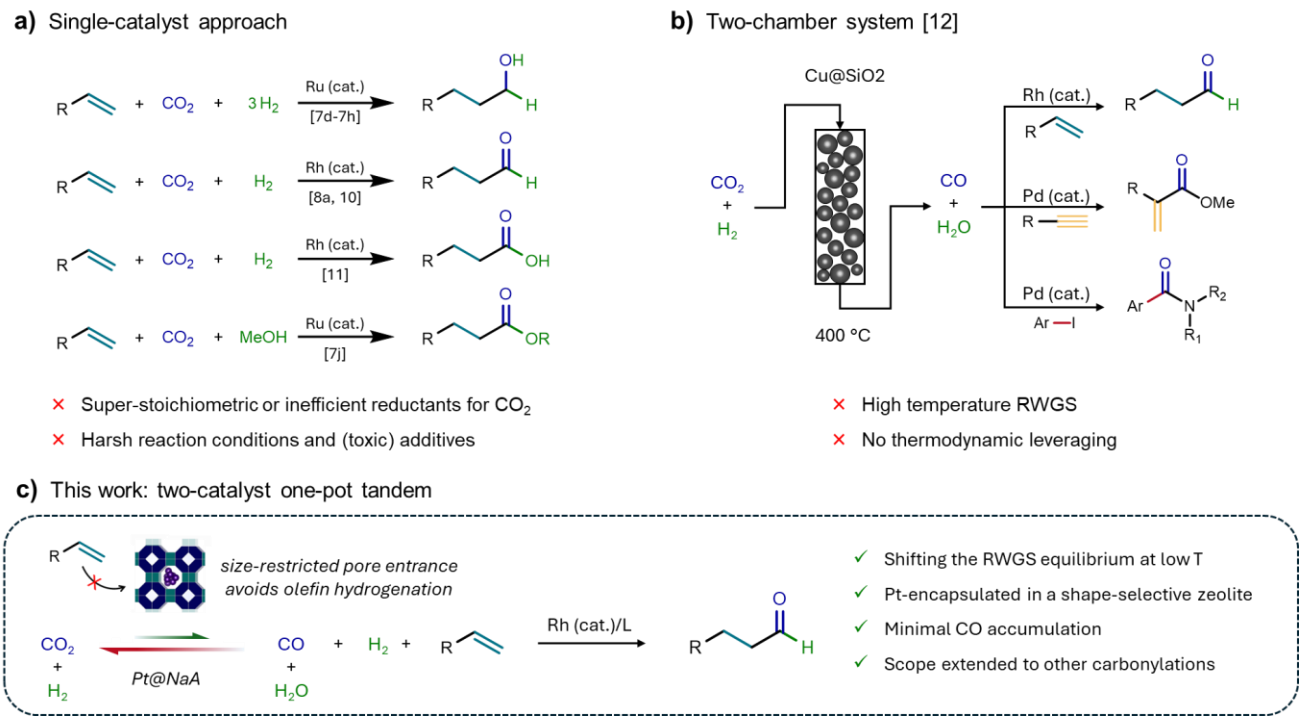

Figure 1. Coupling of CO_2 reduction with carbonylation reactions. a) Single-catalyst approach for functionalization of olefins with CO_2. b) Two-chamber system for coupled RWGS and carbonylation reactions. c) This work: two-catalyst, one-pot tandem, for RWGS equilibrium shifting by consecutive carbonylation reactions.

disclosed a Rh-PPh_3 system to promote both the RWGS and the carbonylation in the hydrocarboxylation of olefins for an atom-economical production of the corresponding acids.[11] Nevertheless, one-catalyst strategies often result in a sub-optimal outcome for both RWGS and carbonylation, and thus, the overall reaction. Alternatively, a "two-chamber" system has been proposed by Beller (Figure 1b), in which the CO-generating and CO-consuming reaction are spatially separated, underlining the incompatibility of both reactions.[12] Although both reactions were performed with specialized catalysts under ideal conditions, this approach does not overcome the thermodynamic restrictions imposed by the equilibrium-limited endothermic RWGS. Clearly, a truly simultaneous CO-generation (RWGS) and consecutive (exothermic) CO-consuming *in situ* reaction are required to leverage the thermodynamics of coupled reactions (Figure 1c).[13] Moreover, the continuous consumption of the toxic CO at low partial pressures reduces its accumulation, minimizing risks in industrial operation.

In light of this, we herein propose a physical isolation of the RWGS-function from the carbonylation function in a one-pot system (Figure 1c). This compartmentalization is achieved through the spatial confinement of a noble metal in a small-pore zeolite (i.e. an 8MR zeolite), using its molecular sieving effect to limit access to the noble metal active site to only CO_2 and H_2, along with a separate homogeneous catalytic system in one pot. The efficiency of this novel methodology is demonstrated for olefin hydroformylation and extended to other carbonylation reactions using CO_2 and H_2 as the CO-source.

Results and Discussion

Confining the RWGS Function inside a Metal Loaded Small-Pore Zeolite

To enable our compartmentalized approach for olefin functionalization with CO derived from the RWGS reaction, employing a low-temperature RWGS catalyst is essential. We envisage noble metal particles for this purpose as suitable catalysts; thus, entrapment within a microporous environment is crucial to impede the undesired hydrogenation of the olefin reactants. Therefore, we initially explored different synthesis strategies for noble metal particle embedment inside relevant small-pore zeolite hosts (LTA, CHA and AEI topologies; Table S1).[14] Remarkably, a preliminary evaluation of these materials identified noble metals confined in NaA (denoted as M@NaA; LTA topology) as promising catalysts in mild RWGS conditions (Table S2, Figure S1). The effective encapsulation of the metal within the LTA voids was realized through addition of amine-stabilized metal precursors during hydrothermal synthesis. Ultimately, the Pt@NaA catalyst demonstrated the most favourable outcome, with a CO productivity of 3.7 mol CO mol Pt^{-1} h^{-1} at 120 °C in the first 4 h, and a higher content of encapsulated metal compared

to the Rh@NaA catalyst (Figure S2). Critically, Pt@NaA maintained similar activities in pressurized liquid phase conditions as in solventless conditions (Table S3, Figure S3).

Characterization of the Pt@NaA zeolite catalyst was carried out through a variety of advanced techniques. Using inductively coupled plasma optical emission spectroscopy analysis (ICP-OES), the optimal catalyst was found to contain 0.75 wt.% Pt. Powder X-ray diffraction (PXRD) disclosed the highly crystalline nature of the zeolite catalyst, with no observable peaks in the diffractogram that could be assigned to metallic Pt phases (Figure S4). Additionally, ^{27}Al and ^{29}Si MAS NMR spectra exhibited the framework stability of the Pt@NaA zeolite catalyst under reaction conditions (Figure S5). Cubic-shaped zeolite crystallites, typical for LTA, of 300-500 nm were observed from secondary electron images with a scanning transmission electron microscope (STEM, Figure S6). Furthermore, the mainly intraporous location of Pt was evidenced by a series of tilt images (Supplementary Video 1). N_2 physisorption isotherms collected at 77 K (Figure S7) were used to analyze the Brunauer-Emmett-Teller (BET) area, which amounted to 8 m^2/g, resulting in an average crystallite size estimate of 450 nm.[15] Furthermore, CO_2-adsorption at 273 K indicated no loss in adsorption capacity of the loaded zeolite in comparison to the parent material, due to metal encapsulation (Figure S8). H_2-chemisorption data of the reduced Pt@NaA sample at 313 K demonstrated a good metal dispersion of 75%, with an average Pt particle diameter of 1.5 nm. The average particle size was confirmed by transmission electron microscopy (TEM) images (1.5 nm, Figure 2a) and by analysis of the Pt-Pt coordination number by extended X-ray absorption fine structure (1.2 nm, EXAFS), assuming ideal spherical shape of fcc-structured Pt particles, based on the average Pt–Pt coordination number (Table S4).[16]

In situ X-ray absorption spectroscopy (XAS) experiments were then carried out to study the evolution of the oxidation state and local structure of the Pt species in Pt@NaA, as a function of the external conditions. The initial state of Pt in the as-synthesized catalyst is identical to that of the original amine-stabilized metal precursor, $Pt(NH_3)_4(NO_3)_2$, in both X-ray absorption near edge structure (XANES) and EXAFS regions (Figure 2b,c), having similar first-shell parameters (Table S4), which confirms the stability of the precursor during the zeolite synthesis. After calcination, the XANES spectrum of the Pt species in the zeolite is similar to that of Pt(IV) oxide (reference sample) (Figure 2b), with the sample lacking higher shell contributions in its EXAFS spectrum (Figure 2c), indicating nanometric dimensions of the Pt(IV) particles (Figure S9-S10). During thermal treatment in H_2, a monotonous reduction from Pt(IV) to Pt(0) is observed (Figure S11). The first-shell Pt–Pt contribution in comparison with Pt foil is characterized by a significantly smaller coordination number, higher disorder and shorter interatomic distance (Table S4), all indicative of the nanometric (ca. 1.2 nm) dimensions of Pt(0) particles. During in situ XAS measurements under RWGS conditions, the Pt nanoparticles remain stable in their metallic state (Figure S12), while generation of CO is observed via mass spectrometry. A slight increase of the white line is already observed at 50 °C and remains up to 120 °C, which may be explained by an electron transfer from Pt nanoparticles to surface adsorbates.

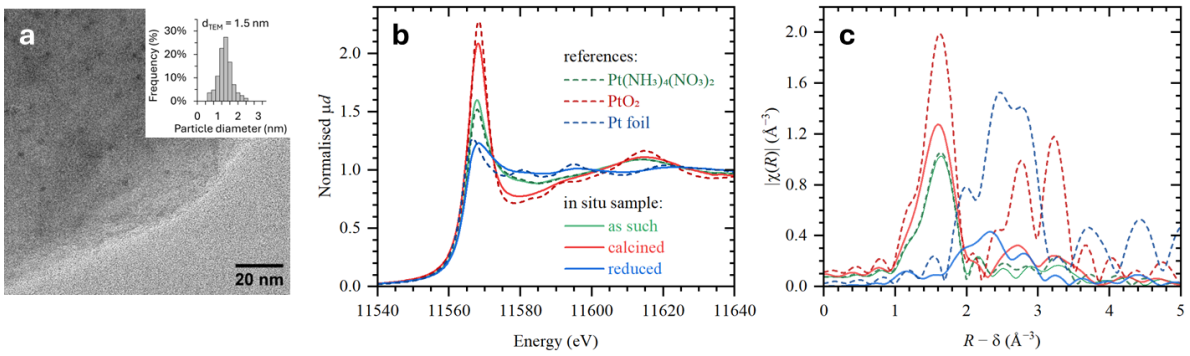

Figure 2. Characterization of the Pt@NaA zeolite. a) TEM image of Pt nanoparticles and metal cluster size distribution of Pt@NaA. b), c) Steady-state XANES (b) and EXAFS (c) spectra of the sample in its as-synthesized form (solid green), after calcination (solid red) and subsequent reduction (solid blue) with reference spectra (dashed lines)

Coupling the RWGS with Olefin Hydroformylation

As a starting point for the one-pot RWGS-hydroformylation reaction, 195 mg of the Pt@NaA catalyst (2.5 mol% Pt; RWGS function) was submerged in dry toluene in combination with 0.267 mol% $Rh(acac)(CO)_2$ and a selection of phosphorous containing ligands for the hydroformylation of 1 octene (0.2 M; **1a**) to nonanal (**2a**) (Table 1). To our delight, the use of 3,7-diacetyl-1,3,7-triaza-5-phosphabicyclo[3.3.1]nonane (DAPTA, entry 1, **L1**) as a ligand for the one-pot hydroformylation with 15 bar CO_2 and 5 bar H_2 at 120 °C, resulted in a remarkable **2a** yield of 70% with high regioselectivity (l:b=96:4) after 20 h of reaction time. Interestingly, limited olefin hydrogenation (6%) was observed, while the RWGS activity was preserved when combining both catalysts, hinting towards an effective Pt encapsulation. Notably, the structurally similar PTA ligand (Table 1, entry 2, **L2**), which was used in the

Table 1. Ligand screening for the hydroformylation of **1a** with CO_2 and H_2.[a]

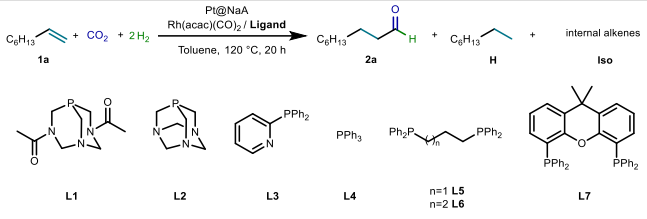

Entry	Ligand	Yield **2a** (%)	Yield H (%)	Yield Iso (%)
1	**L1**	**70 (96:4)** [b]	**6**	**12**
2	L2	8 (88:12)	6	11
3	L3	-	53	43
4	L4	-	30	57

5	L5	17 (99:1)	46	35
6	L6	7 (99:1)	67	24
7	L7	-	97	2

[a] Reaction conditions: 1-octene (0.3 mmol), Pt@NaA (195 mg, 2.5 mol%), $Rh(acac)(CO)_2$ (0.8 µmol, 0.267 mol%), P/Rh = 20, dry toluene (1.5 mL), 15 bar CO_2, 5 bar H_2, 120 °C, 20 h. [b] The regioselectivity is shown in the parentheses.

single-catalyst CO_2 hydroformylation of olefins with acetic anhydride as crucial additive,[9] showed a low hydrogenation activity, comparable to that obtained with **L1**; however, employing this ligand resulted in a low hydroformylation rate, under these conditions. Conversely, for other classic carbonylation ligands, mostly hydrogenation of **1a** was observed with little to no hydroformylation (entries 3-7). Additional control experiments were conducted to validate the need of a two catalyst approach (Table S5). In absence of either the zeolite RWGS catalyst or the homogeneous catalyst complex, no hydroformylation was observed. Additionally, omitting either H_2 or CO_2 from the reaction conditions resulted in no CO formation, nor in formation of hydroformylation products.

To synchronize the rate of CO generation (by the zeolite catalyst) and the rate of carbonylation (by the homogeneous catalyst), the effect of several reaction parameters was studied, including the ligand loading, reaction temperature, CO_2 and H_2 partial pressures, concentration of the olefin, Rh-loading and amount of zeolite (Table S6-S11). Notably, the ligand to Rh ratio was found to be a chemo- and regioselectivity determining factor in this transformation; among the studied conditions, a **L1** to Rh ratio of 20 was found to be optimal. At these relatively high ligand loadings, olefin coordination is likely hindered, suppressing the hydrogenation and isomerisation activity by coordinatively saturating the homogeneous catalyst. Counterintuitively, no surge in hydrogenation activity was observed for an increased amount of the Pt-loaded zeolite. Rather, a decrease in hydrogenation was detected, attributed to an effective entrapment of the metal, and to the increased CO-generation and ensuing olefin carbonylation.

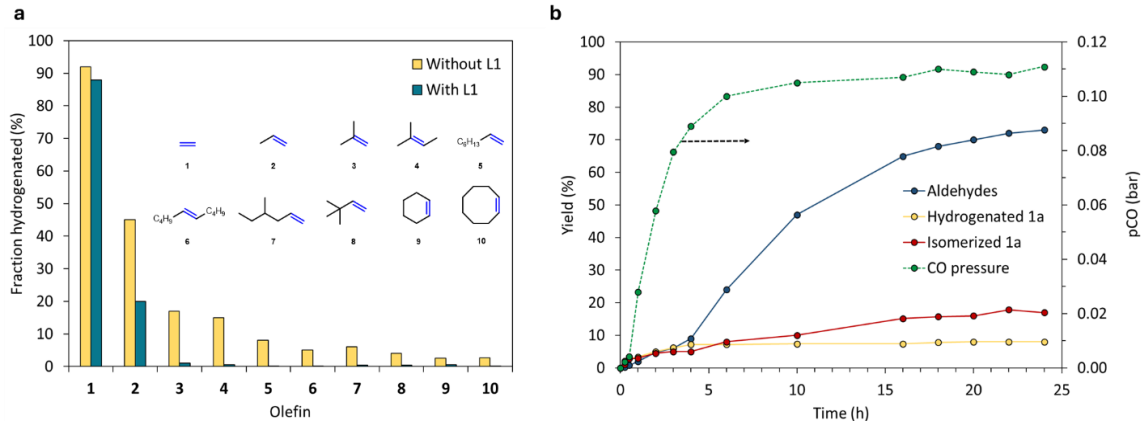

Figure 3. a One-pot RWGS-hydroformylation of olefins with CO_2 and H_2. a) Role of the ligand in suppressing the olefin hydrogenation. Reaction conditions: 0.3 mmol olefin, **L1** = 0 or 16 µmol, 195 mg Pt@NaA (2.5 mol% Pt), 1.5 mL dry toluene, 15 bar CO_2, 5 bar H_2, 120 °C, 2 h. b) Time profile of the yield and partial CO pressure for reaction of **1a** in standard reaction conditions (Table 1).

The inability of the Pt-loaded zeolite to hydrogenate most olefins is further evidenced in Figure 3a. While ethylene (**1**) and to a lesser extent propylene (**2**) were quickly hydrogenated under the imposed conditions, introducing branching (e.g. **3**, **4**, **7** and **8**) or increasing the hydrocarbon chain length (e.g. **5** and **6**), clearly lowered the olefin hydrogenation rates; this demonstrates the molecular sieving effect of the 8MR zeolite pores. While for large olefins such as cycloalkenes (**9** and **10**), hydrogenation activity was already low without any ligand, the addition of **L1** further diminished Pt-catalyzed hydrogenation, presumably by poisoning the rare Pt species residing on the zeolite surface, resulting in negligible hydrogenation for olefins such as 1-octene and isobutene. Additionally, using common Pt supported catalysts (e.g. Pt/Al_2O_3) or Pt on a medium (10MR; Pt/TON) or large pore zeolite (12MR; Pt/BEA) resulted in complete hydrogenation of 1-octene in only 2 h of reaction time (Table S12). Monitoring the time course of the one-pot hydroformylation of **1a** with CO_2 and H_2, in the standard conditions presented in Table 1, revealed that the CO pressure reached a steady-state at ~ 0.1 bar after 6 h (Figure 3b). Thus, it appears that hydrogenation of **1a** mostly occurred during the induction time, when the CO concentration in the system was low. Afterwards, hydroformylation strongly prevailed over any additional olefin hydrogenation, resulting in a **2a** yield of 74% after 24 h of reaction time, highlighting the importance of matched rates of CO-generation and consumption. Remarkably, isomerized octene remained relatively unreactive towards hydroformylation and hydrogenation in these conditions, as both rates dropped at higher **1a** conversions. This again confirms the effective encapsulation of the metal in the small-pore zeolite; any residual hydrogenation of **1a** is to be attributed to the homogeneous catalyst, especially in CO-deficient conditions. Interestingly, the equilibrium of the low temperature RWGS is shifted during our one-pot hydroformylation protocol due to continuous CO-consumption. Monitoring the CO shows that the equilibrium partial pressure during reaction amounts to 0.1 bar, corresponding to a maximum amount of 0.05 mmol CO in the reactor; however, at least four times more product was formed under the imposed conditions.

Using the optimized conditions, a range of olefins were subjected to the one-pot hydroformylation protocol with CO_2 and H_2 (Figure 4). Hydroformylation of linear, terminal C4+ olefins (**2a**-**2d**) showed consistent yields of ~70% and high regioselectivity. Upon decreasing the olefin chain length, the hydrogenation can still be kept under control for propylene (**2e**, 17%); however, hydrogenation activity strongly jumps to 85 % for ethylene (**2f**). This small molecule reduces the CO-yield drastically by diffusing into the zeolite pores and competing with CO_2 for hydrogenation. Introducing branching into the aliphatic chain (**2g**-**2i**) resulted in a marked increase in yield, regio- and chemoselectivity, with only 5% and 3% hydrogenation for 4-methyl-1-hexene and 3,3-dimethyl-1-butene, respectively. The reason behind this is twofold: firstly, these sterically hindered olefins are more limited to enter the zeolites pores, and secondly, their coordination to the homogeneous catalyst is more hindered. Similar results were obtained for the hydroformylation of vinylcyclohexane and 4 vinyl-1-cyclohexene (**2j** and **2k**); interestingly, no hydrogenation of the internal double bound was observed for **2k**. For 3-phenyl-1-propene and 4-phenyl-1-butene (**2l** and **2m**), lower yields were achieved with a significant amount of

isomerised, and consequently, less reactive olefin in these conditions. Finally, various functionalized styrenes (**2n**-**2s**) were converted with good yields up to 89% in our catalytic system.

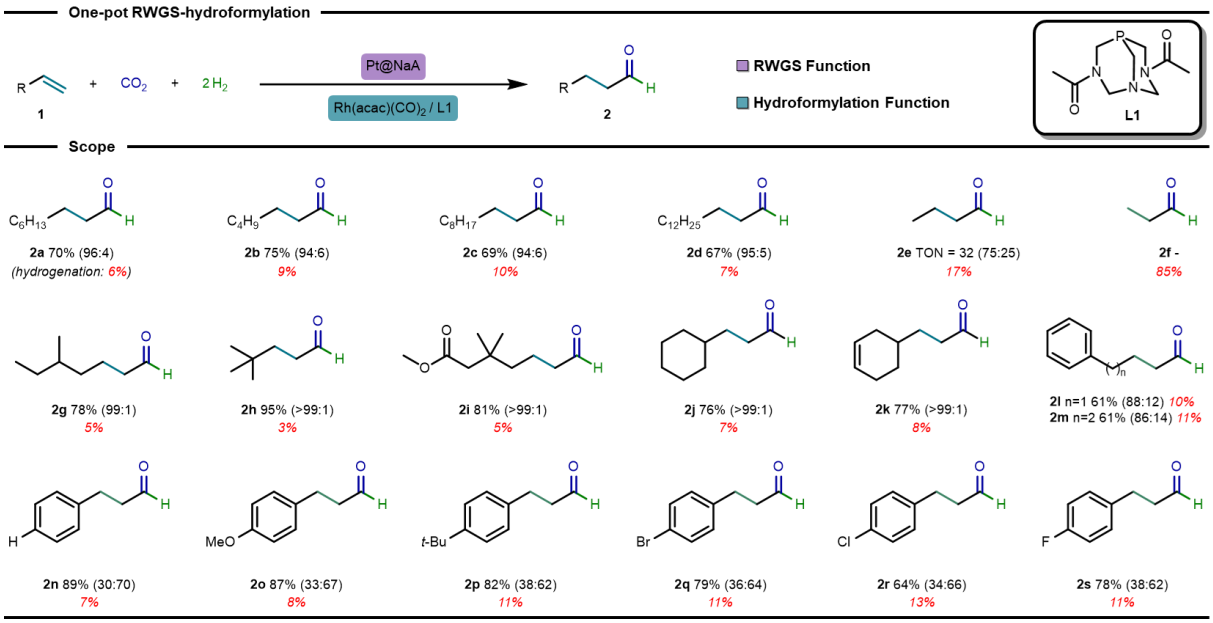

Figure 4. Substrate scope of the one-pot RWGS-hydroformylation with CO_2 and H_2. Reaction conditions: 0.3 mmol olefin, 0.267 mol% $Rh(acac)(CO)_2$, **L1**/Rh = 20, 195 mg Pt@NaA (2.5 mol% Pt), 1.5 mL dry toluene, 15 bar CO_2, 5 bar H2, 120 °C, 20 h. GC-yields using mesitylene as internal standard. Linear to branched ratios are in parentheses, the substrate hydrogenation in red.

Extending the Scope of the Compartmentalized Reaction Concept

With an adequate one-pot CO_2 carbonylation system established, the scientific scope was broadened by exploring different carbonylation reactions. To this end, we directed our focus to the compartmentalized RWGS-aminocarbonylation of aryl bromides, resulting in the formation of benzamides.[17] Initially, the zeolite catalyst, together with Pd_2dba_3 and Xantphos (**L7**) was submerged in the reaction mixture, like in the tandem hydroformylation reaction (*vide supra*). However, only poor yields (34%) were achieved after 24 h of reaction time (Table S13), presumably due to strong adsorption of the amines on the zeolite outer surface. This issue was successfully circumvented by envisioning a different one-pot configuration, in which the zeolite was placed in a basket in the headspace of the reaction vessel, as illustrated in Figure S13.

As a model reaction, the aminocarbonylation of 4-bromoanisole (**3a**) with various amines was considered, optimizing the ratio of the employed catalysts and monitoring the composition of the gas phase (Table S14-S16, Figure S14-S16). Again, the effective formation of the amide product heavily depends on the balance between both reaction rates. Under the studied, uncommonly H_2-rich aminocarbonylation conditions, hydrodehalogenation was observed as the predominant side-reaction. This was attributed to a shortage of CO at unequal reaction rates of the RWGS and aminocarbonylation. Remarkably, under optimized conditions, several aryl bromides reacted smoothly with both primary and secondary amines, resulting in good to excellent yields of amide product (70 to 99%, Figure 5).

Interestingly, the arene with an electron-withdrawing substituent (**3f**) benefitted from a lower Pd loading to compensate for its higher rate of oxidative addition. Finally, the synthesis of a pharmaceutically relevant molecule was successfully achieved with Moclobemide (**4h**), attaining an isolated yield of 92%.

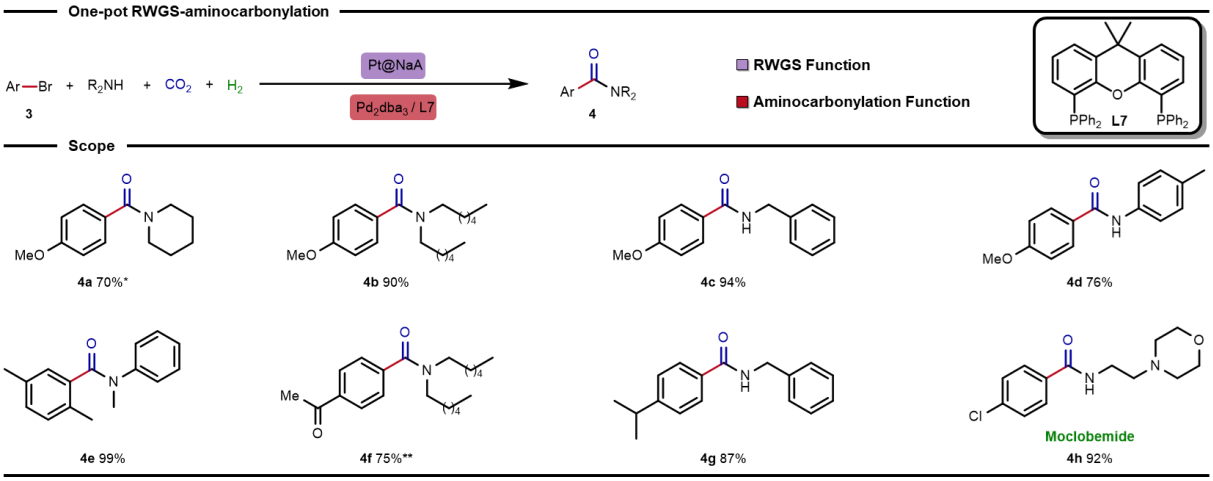

Figure 5. Substrate scope of the one-pot aminocarbonylation with CO_2 and H_2. Reaction conditions: 1.0 mol% Pd (Pd_2dba_3), Pd/**L7** = 1, 800 mg Pt@NaA (6.2 mol% Pt), 0.5 mmol aryl bromide, 1.0 mmol amine, 1.0 mmol Et_3N, 5 mL dry toluene, 15 bar CO_2, 5 bar H_2, 120 °C, 24 h. *2.0 mol% Pd instead. **0.5 mol% Pd instead.

With the revised one-pot CO_2 carbonylation set-up at hand (Figure S13), we were eager to further develop our methodology for other carbonylation reactions. Firstly, we were able to deliver proof-of-concept for the Pd-catalyzed alkoxycarbonylation of olefins, using only CO_2 and H_2 instead of CO (Figure 6a) and 1,2-bis(di-tert-butylphosphinomethyl)benzene (**L9**) as the ligand.[5,18] Both 1-octene (**1a**) and styrene (**1n**) reacted with CO, directly derived from the RWGS, and 3-Me-1 butanol to the corresponding ester in moderate yields, showing the potential of this reaction. Secondly, the reductive carbonylation of 4-bromoanisole efficiently afforded the corresponding aromatic aldehyde (**6**, 78% yield) using CO_2 and H_2 as a source of formyl groups (Figure 6b) with a homogeneous Pd/Cata*CX*ium A (**L10)** system.[19] Lastly, the alkoxycarbonylation of 4-bromoanisole was tested in our compartmentalized protocol (Figure 6c) and resulted in the successful formation of the 2-ethylhexyl ester (**7**) in good yield (67%) with Xantphos (**L7**) as the ligand.[17]

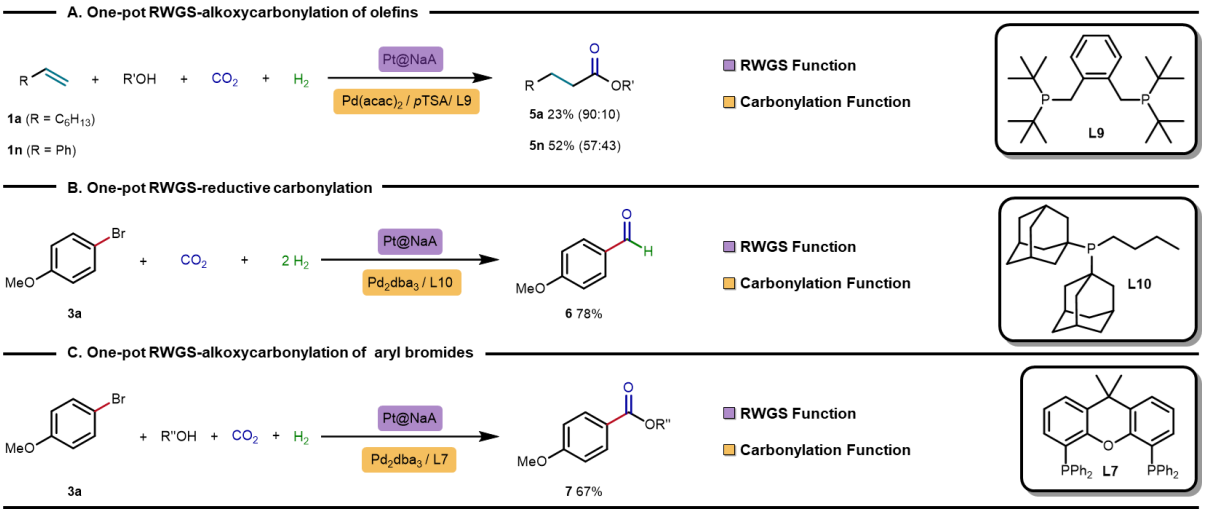

Figure 6. Extended reaction scope of one-pot carbonylation reactions with CO_2 and H_2. Reaction conditions: 800 mg Pt@NaA (6.2 mol% Pt), 15 bar CO_2, 5 bar H_2, 120 °C, 24 h. **A.** 1.5 mol% Pd(acac)2, **L9**/Pd = 4, pTSA/Pd = 16, 0.5 mmol olefin, 5 mL 3 Me-1-butanol (R'OH). Linear to branched ratios are in parentheses. **B.** 0.3 mol% Pd ($Pd_2(dba)_3$), **L10**/Pd = 6, 0.5 mmol 4-bromoanisole, 1.0 mmol Et_3N, 5 mL dry toluene. **C.** 1.0 mol% Pd (Pd_2dba_3), **L7**/Pd = 2, 0.5 mmol 4-bromoanisole, 5.0 mmol 2 ethylhexanol (R''OH), 1.0 mmol Et_3N, 5 mL dry toluene.

Conclusion

Summarizing, we developed a zeolite compartmentalized approach for one-pot carbonylation reactions using CO_2 and H_2 instead of CO. Confined nanoparticles inside a small-pore zeolite were key to impede unwanted olefin hydrogenation, while selectively generating CO in mild conditions. The continuous *in situ* consumption of CO resulted in a reaction equilibrium shift and a minimal accumulation of this toxic gas. Therefore, we provide a promising technology for the incorporation of CO, directly derived from CO_2, in valuable compounds.

Supporting Information

Acknowledgements

We thank C. Marquez and A. Lauwers for help with ICP measurements, J. Vercammen and A. Skorynina for assistance with XAS measurements. H.V.D and S.V.M. thank the FWO for funding (1S31824N, 1SA0921N). Authors acknowledge ReMade project, funded by the European Union as part of the Horizon Europe call HORIZON-INFRA-2021-SERV-01 under grant agreement number 101058414 and co-funded by the Swiss State Secretariat for Education, Research and Innovation (SERI) under contract number 22.00187 for providing access to XAS, TEM and NMR facilities. We

acknowledge the Paul Scherrer Institut, Villigen, Switzerland for provision of synchrotron radiation beamtime at beamline SuperXAS of the SLS. H.V.D. thank VLAIO via the Flemish spearhead cluster Catalisti for financial support (Moonshot cluster SBO project 2CCO2).

Keywords: Carbonylation • CO_2 hydrogenation • Shape-Selectivity • Olefins • Zeolites

[1] a) IPCC, 2023. *Climate Change 2023: Synthesis Report. Contribution of Working Groups I, II and III to the Sixth Assessment Report of the Intergovernmental Panel on Climate Change* [Core Writing Team, H. Lee and J. Romero (Eds.)]. IPCC, Geneva, Switzerland, **2023**; b) N. Mac Dowell, P. S. Fennell, N. Shah, G. C. Maitland, *Nat. Clim. Change* **2017**, 7, 243–249.

[2] a) E. C. Ra, K. Y. Kim, E. H. Kim, H. Lee, K. An, J. S. Lee, *ACS Catal.* **2020**, *10*, 11318–11345; b) J. Artz, T. E. Müller, K. Thenert, J. Kleinekorte, R. Meys, A. Sternberg, A. Bardow, W. Leitner, *Chem. Rev.* **2018**, 118, 434–504; c) B. M. Tackett, E. Gomez, J. G. Chen, *Nat. Catal.* **2019**, *2*, 381–386; d) Q. Liu, L. Wu, R. Jackstell, M. Beller, *Nat. Commun.* **2015**, *6*, 5933.

[3] R. Franke, D. Selent, A. Börner, *Chem. Rev.* **2012**, 112, 5675–5732.

[4] N. Yoneda, S. Kusano, M. Yasui, P. Pujado, S. Wilcher, *Appl. Catal., A* **2001**, 221, 253–265.

[5] J. Vondran, M. R. L. Furst, G. R. Eastham, T. Seidensticker, D. J. Cole-Hamilton, *Chem. Rev.* **2021**, *121*, 6610–6653.

[6] a) S. Kattel, P. Liu, J. G. Chen, *J. Am. Chem. Soc.* **2017**, *139*, 9739–9754; b) A. M. Bahmanpour, M. Signorile, O. Kröcher, *Appl. Catal., B* **2021**, 295, 120319.

[7] a) V. K. Srivastava, P. Eilbracht, *Catal. Commun.* **2009**, *10*, 1791–1795; b) M. Ali, A. Gual, G. Ebeling, J. Dupont, *ChemSusChem* **2016**, *9*, 2129–2134; c) C. Qian, Q. Zheng, J. Ji, G. Liang, B. Tu, T. Tu, *Chem Catal.* **2023**, 3, 100787; d) K.-I. Tominaga, Y. Sasaki, *Catal. Commun.* **2000**, *1*, 1-3; e) K. I. Tominaga, Y. Sasaki, *J. Mol. Catal. A: Chem.* **2004**, 220, 159–165; f) Q. Liu, L. Wu, I. Fleischer, D. Selent, R. Franke, R. Jackstell, M. Beller, *Chem. – Eur. J.* **2014**, *20*, 6888–6894; g) M. Hatanaka, T. Yasuda, E. Uchiage, M. Nishida, K. I. Tominaga, *ACS Sustainable Chem. Eng.* **2021**, 9, 11674–11680; h) Q. Chen, X. Kang, X. Zhang, Y. Cao, L. He, *J. Org. Chem.* **2023**, *88*, 5044–5051; i) S. P. Xia, G. R. Ding, R. Zhang, L. J. Han, B. H. Xu, S. J. Zhang, *Green Chem.* **2021**, *23*, 3073–3080; j) L. Wu, Q. Liu, I. Fleischer, R. Jackstell, M. Beller, *Nat. Commun.* **2014**, 5, 3091.

[8] a) X. Ren, Z. Zheng, L. Zhang, Z. Wang, C. Xia, K. Ding, *Angew. Chem. Int. Ed.* **2017**, *56*, 310–313; b) B. Yu, Z. Yang, Y. Zhao, L. Hao, H. Zhang, X. Gao, B. Han, Z. Liu, *Chem. – Eur. J.* **2016**, *22*, 1097–1102; c) A. G. Wu, J. Ding, L. Zhao, H. R. Li, L. N. He, *ChemSusChem* **2024**, *17*, e202400608; d) S. D. Friis, A. T. Lindhardt, T. Skrydstrup, *Acc. Chem. Res.* **2016**, *49*, 594–605; e) L. Wu, Q. Liu, R. Jackstell, M. Beller, *Angew. Chem. Int. Ed.* **2014**, *53*, 6310–6320; f) X. D. Lang, L. N. He, *ChemSusChem* **2018**, *11*, 2062-2067.

[9] X. He, Y. Cao, X. D. Lang, N. Wang, L. N. He, *ChemSusChem* **2018**, *11*, 3382–3387.

[10] K. Hua, X. Liu, B. Wei, Z. Shao, Y. Deng, L. Zhong, H. Wang, Y. Sun, *Green Chem.* **2021**, 23, 8040–8046.

[11] T. G. Ostapowicz, M. Schmitz, M. Krystof, J. Klankermayer, W. Leitner, *Angew. Chem. Int. Ed.* **2013**, *52*, 12119–12123.

[12] R. Sang, Y. Hu, R. Razzaq, G. Mollaert, H. Atia, U. Bentrup, M. Sharif, H. Neumann, H. Junge, R. Jackstell, B. U. W. Maes, M. Beller, *Nat. Commun.* **2022**, 13, 4432.

[13] a) J. Dallenes, J. Wuyts, N. Van Velthoven, A. Krajnc, G. Mali, O. A. Usoltsev, A. L. Bugaev, D. De Vos, *Nat. Catal.* **2023**, 6, 495–505; b) T. L. Lohr, T. J. Marks, *Nat. Chem.* **2015**, *7*, 477–482.

[14] a) Z. Wu, S. Goel, M. Choi, E. Iglesia, *J. Catal.* **2014**, 311, 458–468; b) M. Moliner, J. E. Gabay, C. E. Kliewer, R. T. Carr, J. Guzman, G. L. Casty, P. Serna, A. Corma, *J. Am. Chem. Soc.* **2016**, *138*, 15743–15750; c) M. Moliner, J. Gabay, C. Kliewer, P. Serna, A. Corma, *ACS Catal.* **2018**, *8*, 9520–9528.

[15] J. Im, H. Shin, H. Jang, H. Kim, M. Choi, *Nat. Commun.* **2014**, *5*, 3370.

[16] A. L. Bugaev, A. A. Guda, K. A. Lomachenko, E. G. Kamyshova, M. A. Soldatov, G. Kaur, S. Øien-ØDegaard, L. Braglia, A. Lazzarini, M. Manzoli, S. Bordiga, U. Olsbye, K. P. Lillerud, A. V. Soldatov, C. Lamberti, *Faraday Discuss.* **2018**, 208, 287–306.

[17] For the amino- and alkoxycarbonylation of aryl bromides with **L7** see e.g. J. R. Martinelli, D. A. Watson, D. M. M. Freckmann, T. E. Barder, S. L. Buchwald, *J. Org. Chem.* **2008**, *73*, 7102–7107.

[18] For the alkoxycarbonylation of olefins with **L9** see e.g. W. Clegg, G. R. Eastham, M. R. J. Elsegood, R. P. Tooze, X. L. Wang, K. Whiston, *Chem. Comm.* **1999**, 1877–1878.

[19] For the reductive carbonylation of aryl bromides with **L10** see e.g. S. Klaus, H. Neumann, A. Zapf, D. Strübing, S. Hübner, J. Almena, T. Riermeier, P. Groß, M. Sarich, W. R. Krahnert, K. Rossen, M. Beller, *Angew. Chem. Int. Ed.* **2005**, *45*, 154–158.

Entry for the Table of Contents

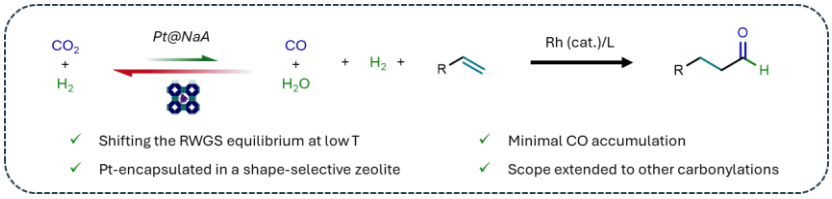

A zeolite-based compartmentalized approach for one-step carbonylation reactions with CO_2 is developed. We show that zeolite shape-selectivity is key to impede unwanted hydrogenation of olefinic substrates and that our catalytic tandem concept enables an equilibrium shift of the low temperature reverse water-gas shift (RWGS) reaction, ultimately resulting in the efficient formation of aldehydes, esters and amides.